Resonant Addressing and Manipulation of Silicon Vacancy Qubits in Silicon Carbide

D. Riedel,[1] F. Fuchs,[1] H. Kraus,[1] S. Väth,[1] A. Sperlich,[1] V. Dyakonov,[1,2] A. A. Soltamova,[3] P. G. Baranov,[3] V. A. Ilyin,[4] and G. V. Astakhov[1,*]

[1]*Experimental Physics VI, Julius-Maximilian University of Würzburg, 97074 Würzburg, Germany*
[2]*Bavarian Center for Applied Energy Research (ZAE Bayern), 97074 Würzburg, Germany*
[3]*Ioffe Physical-Technical Institute, 194021 St. Petersburg, Russia*
[4]*Saint Petersburg Electrotechnical University, 197376 St. Petersburg, Russia*

(Received 7 August 2012; published 27 November 2012)

Several systems in the solid state have been suggested as promising candidates for spin-based quantum information processing. In spite of significant progress during the last decade, there is a search for new systems with higher potential [D. DiVincenzo, Nat. Mater. **9**, 468 (2010)]. We report that silicon vacancy defects in silicon carbide comprise the technological advantages of semiconductor quantum dots and the unique spin properties of the nitrogen-vacancy defects in diamond. Similar to atoms, the silicon vacancy qubits can be controlled under the double radio-optical resonance conditions, allowing for their selective addressing and manipulation. Furthermore, we reveal their long spin memory using pulsed magnetic resonance technique. All these results make silicon vacancy defects in silicon carbide very attractive for quantum applications.

DOI: 10.1103/PhysRevLett.109.226402 PACS numbers: 71.55.−i, 61.72.Hh, 61.72.jd, 76.70.Hb

The double radio-optical resonance in atoms [1] constitutes the basis for an unprecedented level of coherent quantum control. Atomic time standards [2] and multiqubit quantum logic gates [3] are among the most widely known examples. In the solid state, semiconductor quantum dots and the nitrogen-vacancy (NV) defects in diamond, frequently referred to as artificial atoms, are considered as the most promising candidates for quantum information processing [4,5]. Nevertheless, such a high degree of quantum control, as achieved in atoms, has not yet been demonstrated in these systems so far. Therefore, there is a search for quantum systems with even more potential [6].

Recently, intrinsic defects in silicon carbide (SiC) have been proposed as eligible candidates for qubits [7,8]. Indeed, they reveal quantum spin coherence even at room temperature [9–11]. All of these experiments have been carried out under nonresonant optical excitation, where all spins are controlled simultaneously. However, for spin-based information processing it is necessary to perform manipulations of selected spins, while the rest should remain unaffected. This demonstration in SiC is still an outstanding task.

The selective spin control can be realized using a resonant optical excitation. As a rule, inhomogeneous broadening is much larger than the natural spectral linewidth, and such resonant addressing can be done on single centers only. To avoid this problem, we applied a special procedure to "freeze" silicon vacancy (V_{Si}) defects during their growth, allowing us to preserve a high homogeneity inherent to Lely crystals. This is confirmed by the extremely sharp optical resonances in our samples. The spectral width of the V_{Si} absorption lines is several μeV (ca. 1 GHz), which is comparable with that of a single quantum dot or a single NV center in diamond.

We then demonstrate the selective spin initialization and readout by tuning the laser wavelength together with the spin manipulation by means of electron spin resonance (ESR). Such a double radio-optical resonance control indicates that the V_{Si} defects strongly interact with light and are well decoupled from lattice vibrations at low temperatures. The latter is also confirmed by the observation of a long spin-lattice relaxation time ($T_1 = 0.1$ ms). This can be potentially used for the physical implementation of scalable multiqubit quantum logic gates in solid state devices [12], vector magnetometry with nanometer resolution [13], and quantum telecommunications via spin-photon coupling [14].

SiC is a wide-gap semiconductor ($E_g^{6H\text{-SiC}} = 3.05$ eV) and possesses a spectrum of unique mechanical, electrical, and thermophysical properties making it appropriate for many demanding applications [15]. The material properties of SiC, including intrinsic defects, are being investigated for decades. In particular, the V_{Si} defects have been identified in the 1980s [16]. SiC exists in about 250 crystalline forms, called polytypes, which are variations of the same chemical compound that can be viewed as layers stacked in a certain sequence. Here we concentrate on the polytype 6*H*-SiC [see Fig. 1(a)]. It has the stacking sequence *ABCACB* and is characterized by three nonequivalent crystallographic sites, one hexagonal (h) and two quasicubic ($k1$, $k2$).

The investigated 6*H*-SiC samples of high crystalline quality have been grown by the modified Lely method. The high-temperature (2700 °C) seedless crystal growth is driven by the temperature gradients within the crucible, resulting in a pressure gradient and thus, in a mass transport. The process is followed by the subsequent fast cooling, which "freezes" the defects within the lattice at low

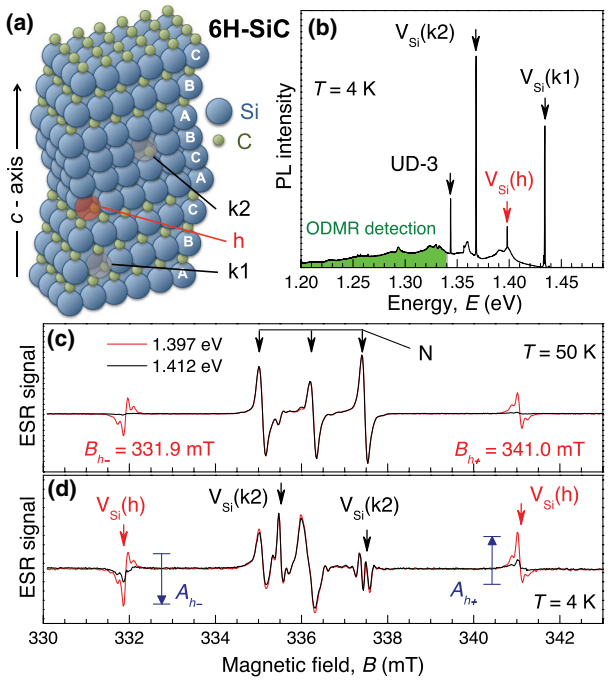

FIG. 1 (color online). (a) The V_{Si} defects present at three nonequivalent crystallographic sites of the 6H-SiC lattice, one hexagonal (h) and two quasicubic ($k1$ and $k2$). (b) PL spectrum obtained under excitation with a He-Ne laser ($E = 1.959$ eV). The ZPLs of the corresponding V_{Si} defects are labeled by arrows. The shaded area from 1.20 to 1.34 eV indicates the spectral range, where the ODMR of Fig. 4 is detected. (c), (d) Light-enhanced ESR under excitation into the $V_{Si}(h)$ ZPL ($E_h = 1.397$ eV) and above-ZPL excitation ($E = 1.412$ eV), recorded at temperatures $T = 50$ and 4 K. The $V_{Si}(h)$ ESR lines are observed at magnetic fields $B_{h-} = 331.9$ mT and $B_{h+} = 341.0$ mT. The ESR experiments are performed in a X-band spectrometer ($\nu_{ESR} = 9.434\,51$ GHz, $B \parallel c$).

densities (for details see Ref. [17]). Taking into account the retrograde character of the nitrogen solubility with temperature, the doping level of the 6H-SiC crystals is below 10^{17} cm^{-3} and the compensation degree of nitrogen donors is ca. 20%. The V_{Si} concentration lies below this value and we estimate that ca. 10^{12} V_{Si} are probed in our experiments.

In all experiments, the samples were mounted in a liquid helium flow cryostat with a temperature controller. Photoluminescence (PL) was excited by a He-Ne laser and detected by a CCD camera linked to a 800-mm monochromator. For the resonance excitation we used a tunable diode laser system with a linewidth below 1 MHz. The ESR experiments were performed in a home-modified X-band spectrometer, with the magnetic field applied parallel to the c axis of 6H-SiC. The magnetic field inside the spectrometer was modulated at a frequency of 100 kHz and the ESR detection was locked-in.

Figure 1(b) presents a typical low-temperature ($T = 4$K) photoluminescence (PL) spectrum of our 6H-SiC sample obtained with sub-bandgap excitation with a HeNe laser ($E = 1.959$ eV). The PL consists of sharp zero phonon lines (ZPLs) and their sideband phonon replicas. Three of these ZPLs—labeled as $V_{Si}(h)$, $V_{Si}(k1)$ and $V_{Si}(k2)$—originate from silicon vacancies at the corresponding crystallographic sites [18]. The origin of the UD-3 ZPL is still under debate [19], and we do not discuss it in what follows.

We now present light-enhanced ESR experiments. It has been shown that the ground state of silicon vacancies is a high-spin state [20]. In 6H-SiC with hexagonal crystal structure the V_{Si} defects have the point group symmetry C_{3V}, allowing for a zero-field spin splitting (Δ). The application of an external magnetic field leads to a further splitting of the V_{Si} ground state. When the difference between spin-split sublevels meets the ESR frequency (ν_{ESR}) the electron spin resonance occurs. The energy diagrams describing the optical transitions, the spin pumping scheme and the related radio frequency (rf) transitions with respect to the multiplicity of the ground state are discussed in Ref. [21]. In case of the silicon vacancy, two ESR lines should appear for each V_{Si} site at magnetic fields B_- and B_+ [8,21]. If the external magnetic field is applied parallel to the c axis of 6H-SiC, there is the following interconnection between $B_\pm$, ν_{ESR} and Δ

$$h\nu_{ESR} = \mp\Delta + g_e\mu_B B_\pm. \quad (1)$$

Here, $g_e = 2.0$ is the electron g factor and $\mu_B = 5.79 \times 10^{-5}$ eV/T is the Bohr magneton. The amplitudes ($A_\pm$) of the V_{Si} ESR lines depend on the population difference between the particular spin sublevels involved. In the dark the difference is due to the Boltzmann factor and the amplitudes $A_\pm$ are negligibly small. The optical excitation of V_{Si} defects and following relaxation preferentially pump the system into certain spin sublevels of the V_{Si} ground state. This results in light-enhanced ESR, as exactly observed in our experiments presented in Figs. 1(c) and 1(d).

First, we discuss the high temperature data [Fig. 1(c)]. The three lines in the magnetic field range from 335.0 to 337.5 mT are the well known ESR fingerprint of the nitrogen (N) donor in 6H-SiC [15], being independent of the optical excitation. The pair of outer lines at magnetic fields $B_{h-} = 331.9$ mT and $B_{h+} = 341.0$ mT appears in the ESR spectrum under optical excitation into the $V_{Si}(h)$ ZPL ($E_h = 1.397$ eV). Using Eq. (1) we obtain the zero-field spin splitting in the $V_{Si}(h)$ defect $\Delta_h = 0.527$ μeV (127 MHz), which is in agreement with the earlier reported value [22].

At cryogenic temperatures, the $V_{Si}(h)$ ESR lines are also observed under the above-ZPL excitation ($E = 1.412$ eV), as shown in Fig. 1(d). In addition, the pair of $V_{Si}(k2)$ resonances appears. Again using Eq. (1) we obtain the zero-field spin splitting in the $V_{Si}(k2)$ defect $\Delta_{k2} = 0.11$ μeV (27 MHz) [22].

Remarkably, under optical excitation the B_+ and B_--lines of V_{Si} (both h and $k2$) have opposite phase in ESR spectra. This is a signature of the spin pumping under

optical excitation, leading to an inverse population between spin sublevels. As a result, rf emission rather than absorption is detected for one of these ESR lines [21]. For $V_{Si}(h)$ the rf emission is observed at the magnetic field B_{h-}, as schematically indicated in Fig. 1(d). For convenience we assume a positive value for the absorbing resonances ($A_{h+} > 0$) and a negative value for the emitting resonances ($A_{h-} < 0$).

Figure 2(a) shows how $A_{h\pm}$ depend on the excitation energy. For energies $E < E_h$ the spin pumping is inefficient, for $E > E_h$ it growths monotonically, presumably due to phonon-assisted processes and for $E = E_h$ a very sharp optical resonance is detected. A similar behavior is observed for A_{k2-} with $E = E_{k2}$ [Fig. 2(b)].

We are now in the position to discuss the double radio-optical resonance of $V_{Si}(h)$. The ESR signal as a function of the relative magnetic field B-B_{h-} and relative excitation energy E-E_h is presented in Fig. 2(c). One can relate the ESR satellites at B-$B_{h-} = \pm 0.17$ mT and ± 0.34 mT to one and two nuclear spin-carrying isotopes ^{29}Si ($I = 1/2$) among the 12 next-nearest-neighbor silicon atoms [Fig. 2(d)]. The optical resonance reveals a complex structure consisting of a series of extremely sharp lines. It is more clearly seen in Fig. 3(a), where the $V_{Si}(h)$ optical resonance from Fig. 2(a) is shown with higher resolution. Remarkably, the spectral width of an isolated line is about 2 μeV [the inset of Fig. 3(a)], which is comparable with the typical spectral linewidth of single defects [23]. We ascribe these results to different areas

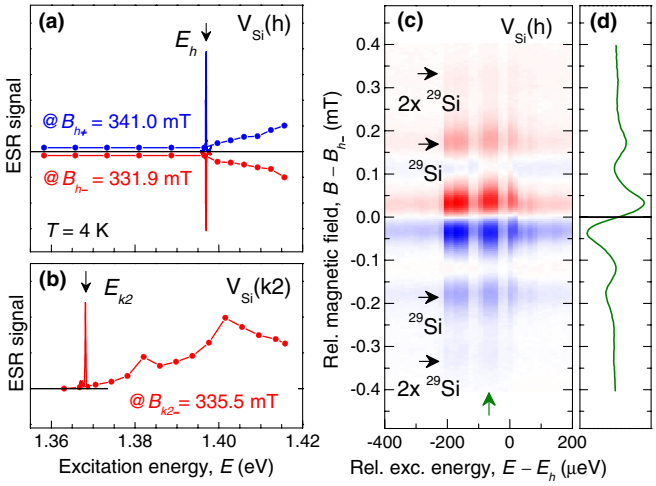

FIG. 2 (color online). (a) The peak-to-peak values $A_{h\pm}$ of the $V_{Si}(h)$ ESR lines [see Fig. 1(c)] recorded in magnetic fields $B_{h-} = 331.9$ mT and $B_{h+} = 341.0$ mT as a function of the excitation energy. (b) The same as (a), but for A_{k2-} recorded in a magnetic field $B_{k2-} = 335.5$ mT. (c) A 2D color plot of the ESR signal as a function of the relative magnetic field B-B_{h-} and the relative excitation energy E-E_h. Here, $B_{h-} = 331.9$ mT and $E_h = 1.397$ eV correspond to the ESR and optical resonance of the $V_{Si}(h)$ defect, respectively. (d) A cross section of c at E-$E_h = -79$ μeV (as indicated by the vertical arrow).

within our SiC crystal, having slightly varied ZPL energies due to different local environment.

Based on the data of Figs. 2 and 3(a) an important conclusion can be drawn: the $V_{Si}(h)$ spins are only addressed when the optical resonance and ESR conditions are simultaneously fulfilled. The contrast—i.e., the ratio of the ESR signal between on and off resonant optical excitation—is above 200. No signature of $V_{Si}(h)$ ionization is observed. Such a behavior differs from diamonds, where for the resonant control of NV defects an additional nonresonant illumination is necessary to deshelve the NV defects from the dark state [24]. To the best of our knowledge, in the solid state, similar double radio-optical resonance has only been observed in quantum dots so far [25].

We now discuss the efficiency of the optical resonance pumping. The $A_{h\pm}$ dependence on the excitation power density P is presented in Fig. 3(c). In the range of P under study we observe $A_{h-} \approx -A_{h+}$, meaning that the photo-induced spin polarization is significantly larger than that due to the Boltzmann statistics. The experimental data can be well described by a standard model for spin pumping, which was initially applied for atoms [21,26]

$$A_{h\pm} \approx \pm A_h = \pm A_{h0} \frac{1}{1 + P_0/P}. \quad (2)$$

Here, $P_0 = 2.62$ W/cm^2 is a characteristic power density obtained in time-resolved experiments as described later. A phonon-assisted spin pumping with the excitation energy 15 meV above the ZPL is less efficient and for $P <$ 1 W/cm^2 linearly depends on the laser power density.

With rising temperature, the resonance spin pumping is observed up to 50 K [Fig. 3(d)]. Remarkably, at $T = 50$ K the multiple-line structure is not resolved any more, but the contrast still remains the same [Fig. 3(b)]. The suppression above 50 K is accompanied by the increase of sample conductivity due to the ionization of nitrogen donors. The conductivity is probably the only limiting factor, as in insulating SiC samples the spin pumping is efficient even at room temperature [11].

We now discuss possible applications of the double radio-optical resonance in SiC. Due to the local environment, the optical resonance and ESR energies are individual for each defect. Additionally, they can be changed by a local electric or magnetic field in the range of 50 μeV [23,27,28]. This can eventually provide a spectroscopic tool to selectively address and manipulate entangled V_{Si} qubits by varying the excitation energy or alternatively by tuning the double radio-optical resonance conditions for a given V_{Si} qubit.

The demonstrative experiments are performed using the optically detected magnetic resonance (ODMR) technique, which can be sensitive to a single defect spin [29]. The ODMR signal is obtained as a normalized change in photoluminescence ΔPL/PL of the sideband phonon replicas, as indicated in Fig. 1(b). We note that the V_{Si}-related PL is observed even at room temperature. In the ODMR

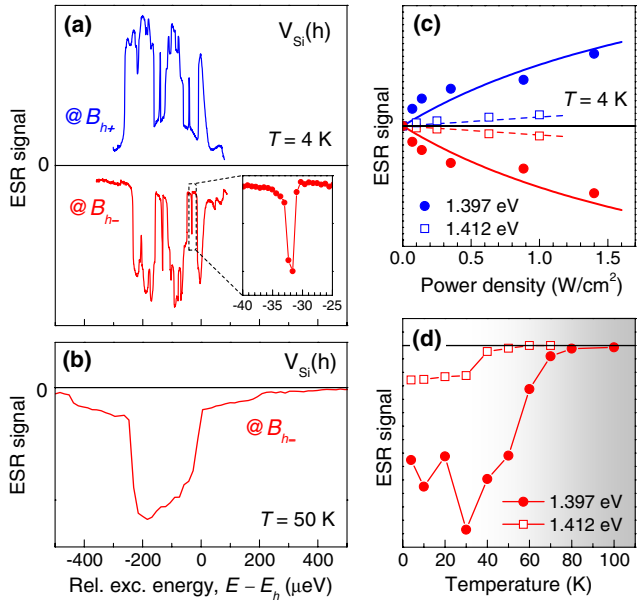

FIG. 3 (color online). (a),(b) The same as in Fig. 2(a), but recorded in the vicinity of E_h with higher spectral resolution at different temperatures. (c) The peak-to-peak values $A_{h\pm}$ of the $V_{Si}(h)$ ESR lines recorded in magnetic fields B_{h-} and B_{h+} as a function of excitation power density. The solid lines are fits to Eq. (2). The dashed lines are linear fits. (d) The peak-to-peak values $A_{h\pm}$ under excitation into the ZPL (E_h = 1.397 eV) and above-ZPL excitation (E = 1.412 eV) as a function of temperature. With rising temperature the SiC sample starts impending the ESR detection in the gray shaded temperature region.

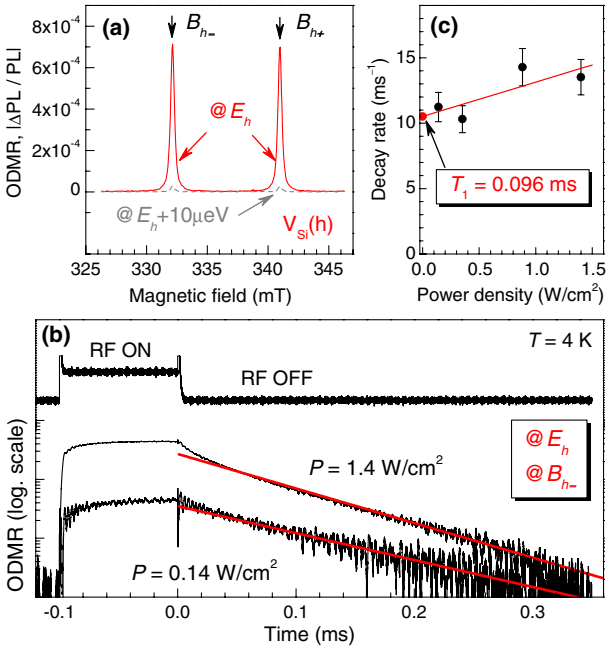

FIG. 4 (color online). (a) ODMR spectra, obtained under optical excitation with the energy of the $V_{Si}(h)$ transition E_h = 1.397 eV and with a slightly detuned energy $E = E_h + 10\ \mu$eV. $B \parallel c$. (b) Time-resolved ODMR signal (the lower curves) recorded after a rf pulse (the upper curve) under the double spin resonance condition, i.e., with an excitation energy E_h and in a magnetic field B_{h-}. The thick solid lines represent exponential fits $A_h \exp(-\alpha t)$ for two excitation power densities P = 1.4 and 0.14 W/cm^2. (c) Decay rate α as a function of P. A linear extrapolation to $P = 0$ yields the spin-lattice relaxation time $T_1 = 0.096 \pm 0.011$ ms.

experiments the PL was passed through a 925 nm long pass filter and detected by a Si photodiode. In order to improve the signal-to-noise ratio the rf was modulated on and off at a frequency of 4.2 kHz and the photovoltage was locked-in.

Figure 4(a) shows ΔPL/PL as a function of the magnetic field obtained under resonance excitation with the energy E_h. Two $V_{Si}(h)$ lines are observed at magnetic fields B_{h-} and B_{h+}, similar to the light-enhanced ESR experiments of Fig. 1(c). When the excitation energy is detuned off the optical resonance by only 10 μeV, the ODMR signal is strongly suppressed.

Finally, we measured spin dynamics of $V_{Si}(h)$ under the double radio-optical resonance conditions, i.e., at E_h and B_{h-}. The experimental details are given in the Supplemental Material [21]. In brief, the system is optically pumped with continuous wave excitation. An intense rf pulse equalizes the spin population in the different sublevels. The time evolution of the ODMR signal after the rf pulse follows an exponential decay. Fit examples to $A_h \exp(-\alpha t)$ for different pump power densities P are presented in Fig. 4(b). As can be shown [21], the decay rate α depends on the spin-lattice relaxation time T_1 and the characteristic power density P_0 as

$$\alpha = \frac{1}{T_1}\left(1 + \frac{P}{P_0}\right). \tag{3}$$

A linear extrapolation of $\alpha(P)$ to $P = 0$ yields $T_1 = 0.096 \pm 0.011$ ms [Fig. 4(c)]. This compares reasonably well with that of NV defects in diamonds [30].

Conclusions and outlook.—The silicon vacancy defects in SiC combine the advantages of semiconductor quantum dots and the NV defects in diamond in one system, making them very attractive for quantum spintronics applications. They are well isolated from the SiC lattice, and tunable lasers with a narrow linewidth can be utilized for the double radio-optical resonance coherent control of V_{Si} qubits, by analogy with atoms. Given that silicon and carbon have nuclear spin free isotopes, one would expect extremely long spin coherence in isotopically purified ^{28}Si^{12}C, similar to phosphorous donors in pure ^{28}Si [31]. An important technological aspect of V_{Si} in SiC is their possibility to be created in state-of-the-art transmission electron microscopes [32], suggesting intriguing perspectives for spin engineering. Furthermore, since spatially separated V_{Si} defects can be selectively addressed even within a single SiC nanocrystal, they can be used as a sensitive probe to image magnetic field vectors and field gradients at nanoscale. And last but not least, single V_{Si} centers in SiC are optically active in near infrared, where

the absorption of silica glass fibers is weak. This may allow for the practical realization of quantum communications as silicon vacancies can be incorporated into SiC-based LED structures or SiC-based photonic crystals.

We acknowledge financial support by the Bavarian Ministry of Economic Affairs, Infrastructure, Transport and Technology as well as by the Russian Ministry of Education and Science (Contract No. 16.513.12.3007).

*astakhov@physik.uni-wuerzburg.de

[1] A. Kastler, Science **158**, 214 (1967).
[2] S. A. Diddams, J. C. Bergquist, S. R. Jefferts, and C. W. Oates, Science **306**, 1318 (2004).
[3] B. P. Lanyon, C. Hempel, D. Nigg, M. Müller, R. Gerritsma, F. Zähringer, P. Schindler, J. T. Barreiro, M. Rambach, G. Kirchmair, M. Hennrich, P. Zoller, R. Blatt, and C. F. Roos, Science **334**, 57 (2011).
[4] D. Loss and D. P. DiVincenzo, Phys. Rev. A **57**, 120 (1998).
[5] P. Neumann, N. Mizuochi, F. Rempp, P. Hemmer, H. Watanabe, S. Yamasaki, V. Jacques, T. Gaebel, F. Jelezko, and J. Wrachtrup, Science **320**, 1326 (2008).
[6] D. DiVincenzo, Nat. Mater. **9**, 468 (2010).
[7] J. R. Weber, W. F. Koehl, J. B. Varley, A. Janotti, B. B. Buckley, C. G. Van de Walle, and D. D. Awschalom, Proc. Natl. Acad. Sci. U.S.A. **107**, 8513 (2010).
[8] P. G. Baranov, A. P. Bundakova, A. A. Soltamova, S. B. Orlinskii, I. V. Borovykh, R. Zondervan, R. Verberk, and J. Schmidt, Phys. Rev. B **83**, 125203 (2011).
[9] N. Mizuochi, S. Yamasaki, H. Takizawa, N. Morishita, T. Ohshima, H. Itoh, and J. Isoya, Phys. Rev. B **66**, 235202 (2002).
[10] W. F. Koehl, B. B. Buckley, F. J. Heremans, G. Calusine, and D. D. Awschalom, Nature (London) **479**, 84 (2011).
[11] V. A. Soltamov, A. A. Soltamova, P. G. Baranov, and I. I. Proskuryakov, Phys. Rev. Lett. **108**, 226402 (2012).
[12] A. M. Stoneham, Physics **2**, 34 (2009).
[13] G. Balasubramanian, I. Y. Chan, R. Kolesov, M. Al-Hmoud, J. Tisler, C. Shin, C. Kim, A. Wojcik, P. R. Hemmer, A. Krueger, T. Hanke, A. Leitenstorfer, R. Bratschitsch, F. Jelezko, and J. Wrachtrup, Nature (London) **455**, 648 (2008).
[14] J. Hofmann, M. Krug, N. Ortegel, L. Gerard, M. Weber, W. Rosenfeld, and H. Weinfurter, Science **337**, 72 (2012).
[15] *Silicon Carbide: Volume 1: Growth, Defects, and Novel Applications*, edited by P. Friedrichs, T. Kimoto, L. Ley, and G. Pensl. (Wiley-VCH, Weinheim, 2009).
[16] V. S. Vainer and V. A. Il'in, Sov. Phys. Solid State **23**, 2126 (1981).
[17] Y. M. Tairov and V. F. Tsvetkov, J. Cryst. Growth **43**, 209 (1978).
[18] M. Wagner, B. Magnusson, W. M. Chen, E. Janzén, E. Sörman, C. Hallin, J. L. Lindström, Phys. Rev. B **62**, 16 555 (2000).
[19] M. Wagner, B. Magnusson, W. M. Chen, E. Janzén, Phys. Rev. B **66**, 115204 (2002).
[20] S. B. Orlinski, J. Schmidt, E. N. Mokhov, and P. G. Baranov, Phys. Rev. B **67**, 125207 (2003).
[21] See Supplemental Material at http://link.aps.org/supplemental/10.1103/PhysRevLett.109.226402 for experimental setup and details of model calculations.
[22] H. J. von Bardeleben, J. L. Cantin, I. Vickridge, and G. Battistig, Phys. Rev. B **62**, 10126 (2000).
[23] L. C. Bassett, F. J. Heremans, C. G. Yale, B. B. Buckley, and D. D. Awschalom, Phys. Rev. Lett. **107**, 266403 (2011).
[24] A. Dräbenstedt, L. Fleury, C. Tietz, F. Jelezko, S. Kilin, A. Nizovtzev, and J. Wrachtrup, Phys. Rev. B **60**, 11 503 (1999).
[25] M. Kroner, K. M. Weiss, B. Biedermann, S. Seidl, S. Manus, A. W. Holleitner, A. Badolato, P. M. Petroff, B. D. Gerardot, R. J. Warburton, and K. Karrai, Phys. Rev. Lett. **100**, 156803 (2008).
[26] H. Hoffmann, G. V. Astakhov, T. Kiessling, W. Ossau, G. Karczewski, T. Wojtowicz, J. Kossut, and L. W. Molenkamp, Phys. Rev. B **74**, 073407 (2006).
[27] F. Dolde, H. Fedder, M. W. Doherty, T. Nöbauer, F. Rempp, G. Balasubramanian, T. Wolf, F. Reinhard, L. C. L. Hollenberg, F. Jelezko, and J. Wrachtrup, Nat. Phys. **7**, 459 (2011).
[28] M. S. Grinolds, P. Maletinsky, S. Hong, M. D. Lukin, R. L. Walsworth, and A. Yacoby, Nat. Phys. **7**, 687 (2011).
[29] A. Gruber, A. Dräbenstedt, C. Tietz, L. Fleury, J. Wrachtrup, C. von Borczyskowski, Science **276**, 2012 (1997).
[30] B. Naydenov, F. Dolde, L. T. Hall, C. Shin, H. Fedder, L. C. L. Hollenberg, F. Jelezko, and J. Wrachtrup, Phys. Rev. B **83**, 081201(R) (2011).
[31] A. M. Tyryshkin, S. Tojo, J. J. L. Morton, H. Riemann, N. V. Abrosimov, P. Becker, H.-J. Pohl, Th. Schenkel, M. L. W. Thewalt, K. M. Itoh, and S. A. Lyon, Nat. Mater. **11**, 143 (2012).
[32] J. W. Steeds, G. A. Evans, L. R. Danks, S. Furkert, W. Voegeli, M. M. Ismail, and F. Carosella, Diam. Relat. Mater. **11**, 1923 (2002).